AIAA JOURNAL
Vol. 34, No. 3, March 1996

Initial Experimental Study of Pulsed Electron Beam Fluorescence

F. M. Lutfy* and E. P. Muntz†
University of Southern California, Los Angeles, California 90089

The pulsed electron beam fluorescence technique for the measurement of gas specie densities along with rotational and vibrational population distributions is being developed for use in high enthalpy, chemically reacting flows. The fluorescence generated by a very high current, short duration pulse of energetic electrons is spectroscopically analyzed sufficiently early in the excitation–emission sequence to minimize the effects of collisional quenching and to avoid the subsequent large energy deposition in the gas caused by the beam's electrons. We present the results of both rotational temperature and gas density measurements in static, room temperature nitrogen at pressures between 5 and 150 mtorr. Using a pulsed electron gun as a source, 150-A electron beams with durations of tens of nanoseconds were used to excite fluorescence from nitrogen's first negative system ($N_2^+B^2\Sigma_u^- \rightarrow N_2^+X^2\Sigma_g^+$). The (0, 0) band near 391 nm was observed with a 0.85-m spectrometer for determination of nitrogen rotational temperature and density. The spectrometer's exit slit was modified to enable simultaneous emission intensity measurements in portions of the (0, 0) band's P and R branches. Predicted intensity ratios in the (0, 0) band rotational structure were found to agree with the experimental results. Also, the fluorescent intensity of the (0, 0) band was proportional to the gas density over the range of pressures studied. The initial results reported here are very encouraging and indicate that, with further development, the pulsed electron gun fluorescene technique will provide a powerful new tool for studying nonequilibrium, chemically reacting flows.

Nomenclature

$A_{B\rightarrow X}$	= spontaneous transition probability
$A_{k,l}$	= total spontaneous transition probability to lower state l
$B_{v_1''=0}$	= rotational constant of zeroth vibrational level of the $N_2X^1\Sigma_g^+$ state
C	= mean molecular speed
c	= speed of light
h	= Planck's constant
I_P	= P branch intensity
I_R	= R branch intensity
K	= rotational quantum number without electron spin
k	= Boltzmann's constant
$N(v', K')_0$	= initial number of molecules in the excited state
$N_e(t')$	= number of electrons in beam per unit time
$N_{\text{rate}}(v', t')$	= number of excitations to v' per unit time
$n(v', k', t')$	= excited state population for times after the current pulse
n_g	= test gas number density
$n_k(t_b)$	= excited state population
$n_{\text{rate},0,k}$	= excitation rate per unit volume to the excited state k from initial state 0
$(n''_{K'-1})_{v_1''=0}$	= number density in the $(K'-1)$ rotational level
$(n''_{K'+1})_{v_1''=0}$	= number density in the $(K'+1)$ rotational level
$P(K', K_2'')$	= rotational transition probability for a given K'
P_{k,t_b}	= emitted power observed at time t_b
P_P	= P branch rotational transition probability
P_R	= R branch rotational transition probability
$Q_r(T_r)_{v_1''=0}$	= rotational state sum
$q(v', v_2'')$	= Franck–Condon factor for transition between v' and v_2''
T_r	= rotational temperature
t_b	= time of an assumed uniform beam pulse
t'	= time after attainment of $N(v', K')_0$
$V_e(t')$	= speed of electrons
v'	= vibrational quantum number of $N_2^+B^2\Sigma_u^-$ state
v_1''	= vibrational quantum number of $N_2X^1\Sigma_g^+$ state
v_2''	= vibrational quantum number of $N_2^+X^2\Sigma_g^+$ state
$\nu_{k,l}$	= wave number of the transition
τ	= inverse of the spontaneous transition probability for the v' state
τ_{QC}	= characteristic quenching time
$\Phi(v', K', t')$	= excitation rate to a rotational level K' in the v' state
$\Omega_e(v')$	= excitation cross section for a vibrational level in the v' state
$\Omega_{Q,k}$	= quenching cross section of the state k
$2\tau_b$	= full width at half-maximum of current pulse

Received Feb. 16, 1995; revision received Sept. 15, 1995; accepted for publication Nov. 29, 1995.

*Research Assistant, Aerospace Engineering Department. Student Member AIAA.

†A. B. Freeman Professor, Chairman of Aerospace Engineering Department. Fellow AIAA.

Introduction

SOPHISTICATED computational fluid dynamics simulations are used in the design of high-speed vehicles operating in the hypersonic flight regime (Mach number 10–20). A large portion of the flight envelope of these aircraft/probes involve hypervelocity speeds with associated nonequilibrium flowfield chemistry. There is a critical scarcity of detailed experimental flowfield measurements that can be used to assess the accuracy and validity of flow simulations. A sketch of a test model to be used in the Calspan–University of Buffalo Research Center's (CUBRC) Large Energy National Shock Tunnel (LENS) is shown in Fig. 1 illustrating the installation of a

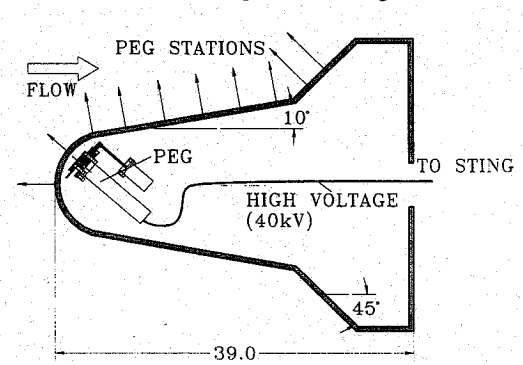

Fig. 1 Pulsed electron gun mounted within test model.

pulsed electron gun for flowfield studies. Electron beam fluorescence (EBF) is a well established and mature diagnostic technique for obtaining density, temperature, internal state population distributions, and velocity measurements at points in low enthalpy gas flows.[1,2] The fluorescent intensity observed from a volume of gas excited by an electron beam can have a linear relationship to gas density below approximately 10^{16} cm^{-3} (300 mtorr at 300 K) (Refs. 3 and 4). At greater densities, collisional quenching causes a nonlinearity between intensity and density, with measurement accuracies becoming increasingly uncertain as the density rises.[1] Since nonequilibrium reacting flow studies must be conducted to quite high densities ($\approx 3 \times 10^{18}$ cm^{-3} for an equivalent altitude of 20 km) (Ref. 5) in the presence of uncertain quantities of quenching species, an alternative to EBF has been proposed: pulsed electron beam fluorescence (PEBF).[5–7]

PEBF retains the advantage of EBF, which is the simultaneous broadband excitation sampling of vibrational and rotational internal energy states of most molecular test species, while making it possible to ameliorate quenching up to number densities of about 10^{18} cm^{-3} (Ref. 7). In addition, background light levels that are the bane of high enthalpy diagnostics are not as problematic since the signal integration time is small. This paper outlines preliminary results using a first-generation pulsed electron gun (PEG) to generate PEBF and measure N_2 density and rotational temperature at pressures between 5 and 150 mtorr in a static cell.

Theory

This discussion briefly highlights PEBF and its quenching avoidance, the relationship between emission intensity and gas number density, and a detailed treatment of rotational temperature measurements. The main features of the PEG are its ability to operate at potentials of order 50 kV and currents between roughly 100–1000 A in extremely short pulses (5–20 ns), resulting in two advantages. First, the short pulse times delay serious complications of quenching up to densities of around 10^{18} cm^{-3}. Second, the elevated current produces a high density of excited states, thereby allowing observation of a strong signal relative to the high background light levels commonly found in high enthalpy flow facilities. The development of pseudospark discharge switches has provided a simple and compact means of generating electron beams with the aforementioned energies and currents (Fig. 2). The PEG operates on the left side of the Paschen curve and is designed to suppress any short path discharges. This forces electrons during a pulsed discharge, which is initiated by a tungsten trigger electrode, to follow field lines that have longer paths between electrodes. As the electrons are accelerated along the field lines, they acquire enough ballistic energy to detach from the field at the exit plane of the gun (Fig. 2). Factors such as distance between electrodes, triggering system, materials, gun chamber gas, and operating potential all impact the performance of pulsed electron guns. These devices produce high-current, self-focusing beams when propagating through higher gas densities, thus maximizing beam collimation.

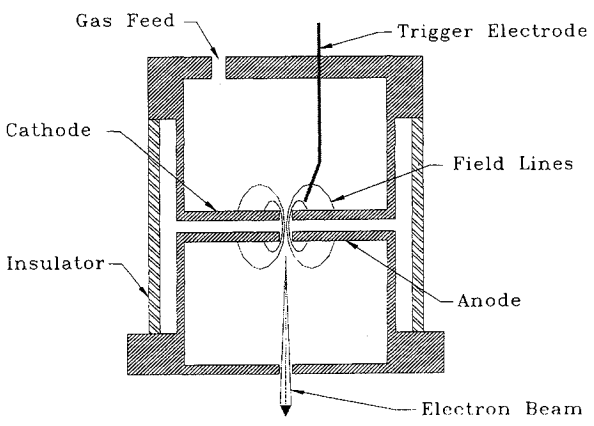

Fig. 2 Schematic of first generation pulsed electron gun.

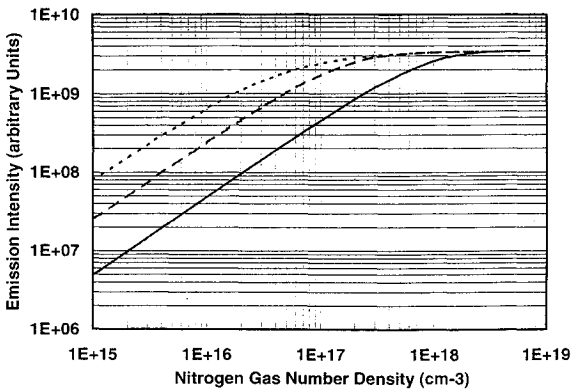

Fig. 3 Quenching curves for different beam pulse lengths: ----, C-W; – – –, t_b = 20 ns; and ——, t_b = 5 ns.

Quenching Avoidance

In this section, the analysis of Ref. 7 is reviewed, showing why PEBF has minimized quenching problems compared to EBF. If $\Omega_{Q,k}$ is the quenching cross section of the state k (15×10^{-16} cm^2 for $N_2^+B^2\Sigma_u^-$, $v' = 0$) and the quenching species number density is defined by n_g, the characteristic quenching time is

$$\tau_{QC} = [C\Omega_{Q,k}n_g]^{-1} \tag{1}$$

where C is the mean molecular speed of the excited species. Following Ref. 7 and considering spontaneous emissions and quenching collisions in a simple three-state system 0, k, l, the time history of the excited state number density becomes

$$n_k(t_b) = \frac{n_{\text{rate},0,k}}{A_{k,l} + C\Omega_{Q,k}n_g}\{1 - \exp[-(A_{k,l} + C\Omega_{Q,k}n_g)t_b]\} \tag{2}$$

Finally, the emitted power that is observed at time t_b because of the excited state population $n_k(t_b)$ is

$$P_{k,t_b} = h\nu_{k,l}A_{k,l}n_k(t_b) \tag{3}$$

Curves given in Fig. 3, which relate P_{k,t_b} to gas density n_Q for three observation times, illustrate the effect of decreasing observation time on increasing the maximum density that can be probed before quenching becomes problematic. It is observed from Eq. (3) and Fig. 3 that for $t_b \to \infty$ (as in the case for continuous wave electron guns used in classic EBF) quenching becomes severe at around 5×10^{16} cm^{-3}. In contrast, the PEG ideally operates on the order of a few nanoseconds (5–20), thereby allowing greater densities to be probed before quenching becomes significant ($\sim 10^{18}$ cm^{-3}).

PEBF and EBF Rotational Fine Structure

Because of the large amount of previous work on EBF rotational intensity distributions,[1,2] it is of interest to relate them to the expected behavior of the PEBF. Consider the transient electron beam excitation of a rotational level in the upper state of nitrogen's first negative system as a result of an electron beam current $I(t')$. If $\Omega_e(v')$ is the excitation cross section for one of the vibrational levels v' of the $N_2^+B^2\Sigma_u^-$ state, the number of excitations to v' per unit time is

$$N_{\text{rate}}(v', t') = \{I(t')/e\}\Omega_e(v')n_g \tag{4}$$

Here, $I(t') = N_e(t')V_e(t')e$ where $N_e(t')$ is the number of electrons in the beam with speed V_e and charge e. The gas number density is n_g and all of the gas molecules will be assumed to be in the ground vibrational state for the purposes of this paper. Following the formalism used by Muntz[1] the excitation rate to a rotational level (K') in the v' state $N_2^+B^2\Sigma_u^-$ is

$$\Phi(v', K', t') = \frac{N_{\text{rate}}(v', t')[H]}{Q_r(T_r)_{v_1''=0}[\Theta]} \tag{5}$$

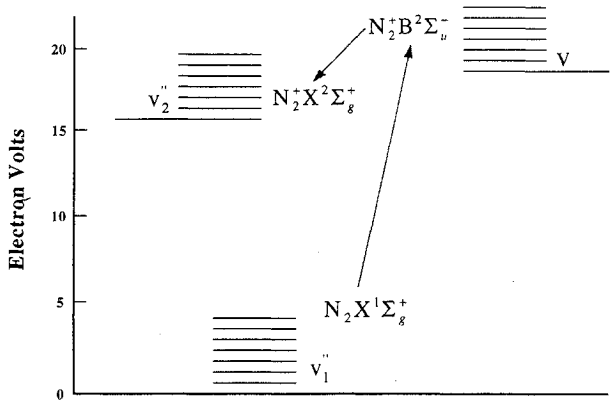

Fig. 4 Excitation diagram for N_2 first negative system.

where v_1'' designates the $N_2X^1\Sigma_g^+$ state and v' the $N_2^+B^2\Sigma_u^-$ state (Fig. 4). $[H]$ and $[\Theta]$ are defined in expressions (6) and (7). Following Muntz,[1]

$$[H] = \left[(K'+1)\exp\left\{-B_{v_1''=0}(K'+1)(K'+2)hc/kT_r\right\}\right.$$
$$\left. + K'\exp\left\{-B_{v_1''=0}(K'-1)K'hc/kT_r\right\}\right] \tag{6}$$

$$[\Theta] = \left[\sum_{K'}\left\{(n''_{K'+1})_{v_1''=0}P_P + (n''_{K'-1})_{v_1''=0}P_R\right\}\right] \tag{7}$$

Assume an electron beam current pulse that is roughly Gaussian with a full width at half-maximum of $2\tau_b$. Also assume a time long enough to include essentially all of the current pulse (i.e., $\pm 3\tau_b$). For these conditions and assuming $\tau_b \ll \tau_{QC}$ with $\tau_b \ll A_{k,l}^{-1}$, an initial number of molecules in the excited state can be defined as $N(v', K')_0$. Neglecting quenching collisions, the excited state population for times after the current pulse is

$$N(v', K', t') = N(v', K')_0 \exp[-t/\tau] \tag{8}$$

where τ is the inverse of the spontaneous transition probability for the v' state of the first negative system having a value of (for $v' = 0$) 6.6×10^{-8} s.

The value of $N(v', K')_0$ can be obtained by integrating Φ over the electron beam pulse width:

$$\int_{-3\tau_b}^{3\tau_b} \Phi(v', K', t')\,dt' \tag{9}$$

The photon emission rate in a rotational line of the v', v_2'' vibrational band of the first negative system as a result of the excited population, assuming a rapid beam pulse and no collisional quenching, is

$$[a(v)]_{K',K_2''} = \frac{N(v')_0 \exp(-t/\tau)A_{B\to X}q(v', v_2'')P(K', K_2'')v^3[H]}{\sum_{v_2''}\sum_{K_2''}\left\{q(v', v_2'')P(K', K_2'')v^3\right\}Q_R(T_R)_{v_1''=0}[\Theta]} \tag{10}$$

where

$$N(v')_0 = \int_{-3\tau_b}^{3\tau_b} \frac{I(t')}{e}\Omega_e(v')n_g\,dt' \tag{11}$$

where v is the wave number. This expression has exactly the same form as the one developed for continuous electron beam excitation of the first negative system[1] as far as the relative intensity distribution in the emission fine structure is concerned. Thus, in deriving information for electron excited intensity measurements in the first negative system's band structure, the earlier work on electron beam fluorescence can be used as an accurate guideline.

Rotational Distribution Measurement

A technique to measure rotational temperature for nitrogen gas was developed in Ref. 8. This approach compares the integrated intensities of carefully chosen sections of an emission band. Specifically, the emission intensity of a piece of the R branch for nitrogen's

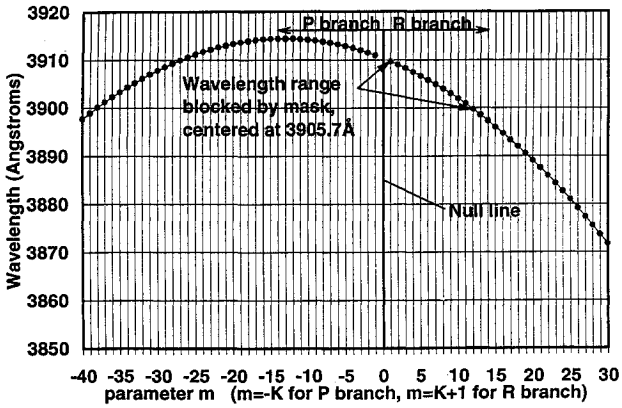

Fig. 5 Rotational wavelength positions; R branch lies right of null line.

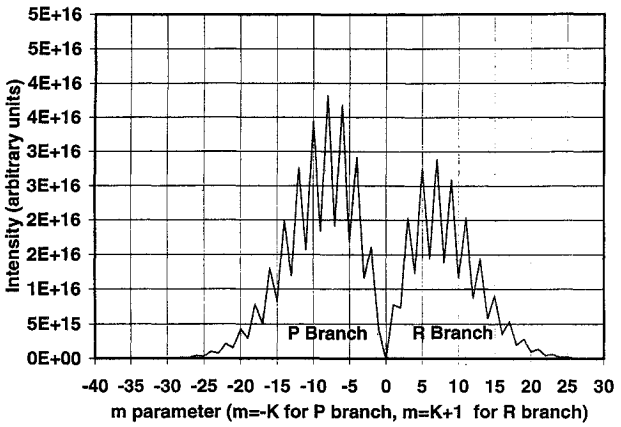

Fig. 6 Intensity distribution of N_2 first negative system (0, 0) band at 300 K.

first negative system (0, 0) band will be divided by the integrated P branch signal. The value of this ratio varies for different rotational temperatures. The emission lines of the rotational fine structure are mapped in a Fortrat parabola in Fig. 5 using the technique outlined in Herzberg.[9] The intensity distribution over K values is found by using the approach in Ref. 8. The R branch will have the following intensity distribution:

$$I_R = 2K'v^4[G]\exp\left\{-\left(B_{v_1''}K'(K'+1)hc/kT_R\right)\right\} \tag{12a}$$

where

$$[G] = \frac{(K'+1)\exp\left\{-2B_{v_1''}(K'+1)hc/kT_R\right\} + K'\exp\left\{2B_{v_1''}K'hc/kT_R\right\}}{2K'+1} \tag{12b}$$

Similarly, the P branch has the following intensity distribution:

$$I_R = 2v^4[G]\exp\left\{-\left(B_{v_1''}K'(K'+1)hc/kT_R\right)\right\} \tag{13a}$$

where

$$[G] = \frac{(K'+1)^2\exp\left\{-2B_{v_1''}(K'+1)hc/kT_R\right\} + K'\exp\left\{2B_{v_1''}K'hc/kT_R\right\}}{2K'+1} \tag{13b}$$

These intensity distributions are presented in Fig. 6 and are quite sensitive to rotational temperature. Therefore, it is possible to determine rotational temperature by comparing the intensities between a carefully picked bandwidth in the R branch with one in the P branch. The R branch bandwidth was chosen to optimize the accuracy of the measurement at the expected rotational temperature. Before ratios between integrated intensities from the bandwidths in

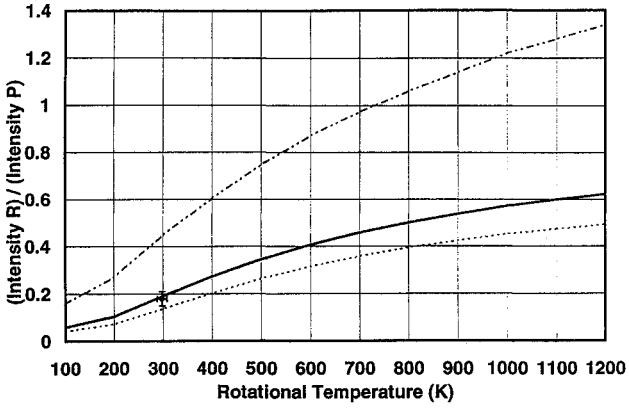

Fig. 7 Integrated intensity ratios for proper spectrometer position (390.57 nm) as well as low and high offset positions and experimental data: ----, −15 nm; – – –, +0.15 nm; ——, 390.57 nm; and •, data.

the R and P branches can be used for temperature measurements, a correction is necessary to account for nuclear spin since in the $N_2X^1\Sigma_g^+$ state, nuclear spin causes the odd-numbered rotational levels ($K'' = 1, 3, 5, \ldots$) to have half the population of the even-numbered ones (Fig. 6). To optimize the accuracy of the measurement, the spectrometer's exit slit was modified to block a portion of the R branch, specifically the K'' values between 0 and 12. Hence, only K'' values of the R branch between 13 and 25 were passed through and divided by the full signal from the P branch. The theoretical integrated intensity ratios as a function of temperature are given in Fig. 7, as well as two curves representing offset positions of ±0.15 nm used to assess the sensitivity of the measurement. The experimental results were compared to these curves to assess any disturbance or optical misalignment introduced to rotational temperature measurement in nitrogen.

Nitrogen Gas Disturbance

There are two processes that potentially could complicate PEBF measurements. First, secondary electrons from ionized nitrogen gas molecules could change the comparative populations of the excited vibrational and rotational states. Some effects on rotation have been observed in EBF, but are not particularly significant at temperatures above 300 K (Ref. 1). The effect of secondary electrons on vibration in EBF is far less well defined. Second, beam energy deposition could heat the nitrogen gas and an artificially high rotational temperature would be detected. Obtaining accurate rotational temperature and number density measurements would alleviate these concerns and significantly increase confidence in the PEBF technique.

Experimental Setup

The purposes of the experiment described in this paper were to study PEBF and to gain some understanding of operational issues associated with PEGs. A schematic of the PEG with supporting apparatus and detection equipment is shown in Fig. 8. The optics focus the electron beam fluorescence within a field of view of about 2 cm at the center of the test chamber. The light is gathered by a collimating lens, reflected from a mirror, and focused at the entrance slit of a SPEX 1404 spectrometer such that the electron beam's image is perpendicular to the entrance slit. The spectrometer has a grating blazed at 500 nm, f/6.9 optics and was operated at an entrance slit setting of 0.4 mm (corresponding to a resolution of 0.12 nm). The exit slit was replaced by an adapter that was fabricated to block off 1.2 nm of wavelength space but allowed 1.7 nm to pass on either side of the center mask. By carefully adjusting the spectrometer's settings (i.e., centered at 390.57 nm), it was possible to pass the P branch while cutting off the aforementioned portions of the R branch. Two 45-deg prisms directed the P and R branch light that diverged from the double exit slit to their respective photomultiplier tubes (PMTs), which have rise times of 2.5 ns. The wavelength calibration of the initial setup was performed using a helium–neon laser and a krypton discharge tube. Since the wavelengths of interest lie between 380.9 and 391.4 nm, it was necessary to ascertain the linear dispersion of the spectrometer at various wavelengths. The

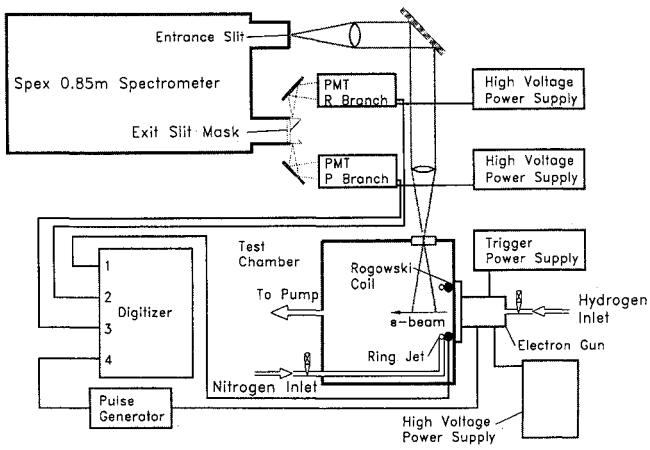

Fig. 8 Experimental setup.

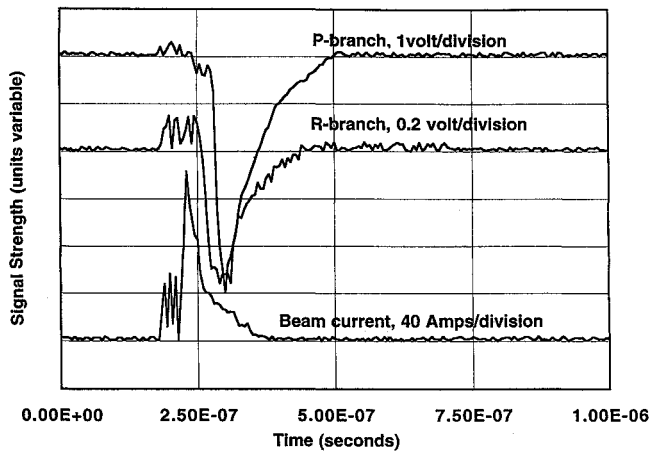

Fig. 9 Digitizer trace of test run at 110 mtorr of N_2.

dispersion was verified to be constant between 632.8 nm (helium–neon laser), 557.028 nm (krypton discharge tube), and 388.865 nm (helium discharge tube). A scaling factor of 2.0 was determined to exist in the PMT signals between the R and P branch channels by viewing the 388.865-nm line of the helium discharge tube. The current measurement was made by a Rogowski coil with a rise time of 20 ns. This coil was placed reasonably close (≈2 cm) to the test chamber viewing area to provide an accurate beam current measurement for the emission volume. Nitrogen was bled through a needle valve and channeled to a ring jet to provide an even gas distribution in the test chamber. The PEG operates in a low-pressure hydrogen environment; the hydrogen was introduced directly into the gun and allowed to escape through the gun orifice and into the vacuum chamber. The pressure was measured using a McLeod gauge and a thermocouple gauge both located close to the optical port. The signals from both PMTs and the Rogowski coil were processed by a Tektronics® TDS-644A digitizer. The pulse generator was a Stanford Research model DG-535. The range of potentials that produced adequate PEG operation lay between 10–33 keV, with typical full width at half-maximum (FWHM) current pulse values of 50 ns, at hydrogen pressures of 100 mtorr. Although the repetition rate of the PEG can be as high as 1.5 Hz, it was consistently operated at 0.2 Hz to prolong the useful life of the trigger electrode. Because the system had no differential pumping ability between the test chamber and PEG, the upper density range of nitrogen that could be explored before contaminating the PEG chamber was 5.3×10^{15} cm^{-3}. The PEG was operated at 33 keV for the experiments presented in this paper. A total of 64 runs were made at pressures varying between 5 and 150 mtorr. Digitizer traces of the two PMT signals and the current for a 110-mtorr pressure run are given in Fig. 9.

Results and Discussion

Because the available first-generation PEG model had only two electrodes and exhibited somewhat erratic triggering, its electron

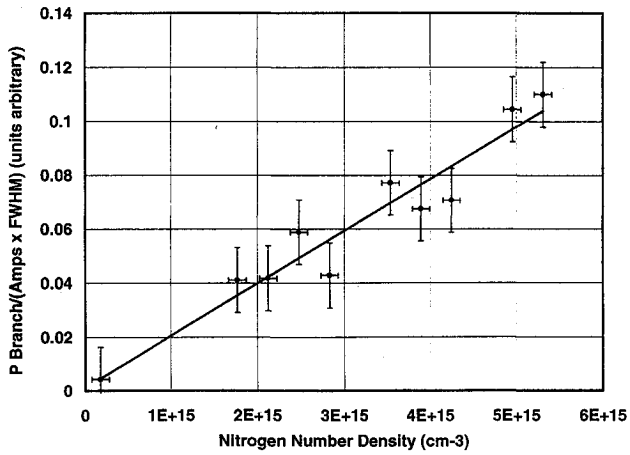

Fig. 10 Linearity verification between emission intensity and N_2 number density.

beam was neither very consistent nor very well collimated. Specifically, the beam's apparent diameter and direction of propagation varied significantly. From shot to shot the beam certainly did not occupy a constant volume within the test chamber, but wandered within and at the edges of the field of view, occasionally exceeding it. The triggering variations caused a shot-to-shot jitter to be as high as ±300 ns. The PEG's instabilities can be remedied by using a multielectrode PEG design.[10,11] The P branch signals for several test chamber densities are shown in Fig. 10 with corresponding 1-sigma error bars. Despite a significant amount of scatter because of the unpredictable firing characteristics of this first-generation PEG, the linear trend is as expected for this pressure range. The rotational temperature was determined by averaging 34 firings. It was necessary to account for the $N_2^+(1, 1)$ band centered at 388.4 nm since it registered within the R branch wavelength range. The theoretical integrated intensity ratios displayed in Fig. 7 include the (1, 1) band contribution. After applying the PMT calibration factor of 2.0, a ratio of 0.18 ± 0.03 was found. As indicated in Fig. 7, this corresponds to a theoretical rotational temperature of 283 ± 30 K. The error specification of ± 30 K represents a 1-sigma spread because of data scatter. Since the nitrogen test gas was at a room temperature of 297 K, the known and measured temperatures are well within experimental uncertainty.

Because of uncertainty in the gun's electron beam energy, it was of interest to compare the observed photon emission rate in the experiments to predicted values using a 33 keV electron beam. All of the following values are approximate estimates. The PMT has a gain of 1.6×10^6 and a quantum efficiency of about 30% at 391.4 nm. For a typical experiment, the P branch channel's measured voltage was 3.5 V, which is equivalent to 2.9×10^{11} photoelectrons/s. The observed photon count entering the PMT is, thus, 1×10^{12}.

Taking into account the limiting solid angle, the spectrometer, reflectance of the mirror, transmission efficiency of the lenses, and the efficiency of the grating, the overall optical transmission of the system was estimated to be 9×10^{-5}. A predicted photon output, after excitation to the $v' = 0$ state of $N_2^+B^2\Sigma_u^-$, can be estimated by integrating an initial population given by Eq. (8) over a typical beam pulse that had 150-A peak current and 50-ns FWHM, or $N(v' = 0)_0 = 5 \times 10^{10}$ excited state $v' = 0$ molecules per unit length of beam. The optical system observed 0.04 cm of beam length and its entire width if the beam was within the field of view, so that the number of emitted photons in the P branch is predicted to be 1.25×10^{16} photons/s. A predicted 1.1×10^{12} photons/s is obtained after applying the optical transmission factor. This is assuming an emission spontaneous transition probability of $A_{B \to X} = 1.24 \times 10^7$ (after Muntz[1]).

The predicted and observed photon counts are in embarrassingly good agreement considering the uncertainty of the many assumptions necessary to generate the comparison. It does indicate that the pulsed electron gun produced beams with energies approaching 33 keV, which was the potential applied to the PEG.

Future Development

Although these preliminary results are encouraging, further development is needed before accurate and dependable measurements can be made in the LENS facility at CUBRC. It is believed that the 1-sigma error bars evident in Fig. 10 can be reduced significantly with a multielectrode PEG design. Utilizing the latter with a pulsed charging system while hardening all electronic equipment against EMI will further enhance the accuracy of single-shot experiments. Temperature measurements in a shock tunnel facility will be accomplished by using an intensified charge-coupled device array in conjunction with a 0.25-m spectrometer. This system will allow observation of a wavelength region approximately 20–40 nm wide. Therefore, the elevated temperatures common to high enthalpy will be determined by slope matching of the acquired emission spectrum with calibrated and theoretical curves.

Conclusions

This paper summarizes a recent experimental investigation of PEBF as a diagnostic technique. An average rotational temperature measurement of 283 K was obtained on a test gas sample that was at room temperature (297 K). In addition, the emission intensity varied approximately linearly with nitrogen pressure. There was significant scatter in the data, undoubtedly because of the inconsistent discharge nature of the present two electrode PEG. It is expected that a multielectrode PEG will overcome the beam quality issues. Estimates of observed photon counts compared to predicted values indicate that the beam energy in the experiment was near the accelerating potential applied to the PEG. The initial results reported here demonstrate that PEBF has the potential of becoming a powerful tool for studying nonequilibrium, high enthalpy flows.

Acknowledgments

This work is supported by the Air Force Office of Scientific Research under University Research Initiative F49620-93-1-0373 with Julian Tishkoff as Grant Monitor. The authors also wish to thank Dan Erwin, Jeff Pobst, and John Schilling for their assistance.

References

[1]Muntz, E. P., "The Electron Beam Fluorescence Technique," AGARDograph 132, Dec. 1968.

[2]Gochberg, L. A., "The Electron Beam Fluorescence Technique in Hypersonic Aerothermodynamics," AIAA Paper 94-2635, June 1994.

[3]Gadamer, E. O., and Schumacher, B. W., "Electron Beam Fluorescence Probe for Measuring the Local Density in a Wide Field of Observation," *Canadian Journal of Physics*, Vol. 36, 1958, p. 659.

[4]Gadamer, E. O., "Measurement of the Density Distribution in a Rarefied Gas Flow Using the Fluorescence Induced by a Thin Electron Beam," Univ. of Toronto Institute of Aerophysics, UTIA Rept. 83, Toronto, ON, Canada, 1962.

[5]Muntz, E. P., Kunc, J. A., and Erwin, D. A., "A Pulsed Electron–Photon Fluorescence Technique for Temperature and Specie Concentration Measurement at Points in Relatively Dense, Unseeded Air Flows," AIAA Paper 87-1526, June 1987.

[6]Schilling, J., Pobst, J., and Erwin, D., "The Use of Pulsed Electron Beam Fluorescence for Arcjet Plume Diagnostics," International Electric Propulsion Conf., IEPC Paper 93-130, Sept. 1993.

[7]Muntz, E. P., and Erwin, D. A., "Rapid Pulse Electron Beam Fluorescence for Flow Field Diagnostics," *New Trends in Instrumentation for Hypersonic Research*, edited by A. Boulier, NATO ASI Series, Series E: Applied Sciences, Vol. 21, Kluwer, Dordrecht, The Netherlands, 1993, p. 265.

[8]Abel, S., and Muntz, E. P., "The Direct Measurement of Static Temperatures in Shock Tunnel Flows," General Electric Technical Information Series R64Sd25, 1964.

[9]Herzberg, G., *Spectra of Diatomic Molecules*, Van Nostrand Reinhold, Scarborough, ON, Canada, 1950, pp. 42–50.

[10]Benker, W., Christiansen, J., Frank, K., Gundel, H., Hartmann, W., Redel, T., and Stetter, M., "Generation of Intense Pulsed Electron Beams by the Pseudospark Discharge," *IEEE Transactions on Plasma Science*, Vol. 17, No. 5, 1989, pp. 754–757.

[11]Frank, K., and Christiansen, J., "The Fundamentals of the Pseudospark and its Applications," *IEEE Transactions on Plasma Science*, Vol. 17, No. 5, 1989, pp. 748–753.